Pergamon

Tetrahedron 56 (2000) 6753–6771

TETRAHEDRON

Site Selective Processes: A Combined Theoretical and Experimental Investigation of Thermally Activated Tautomerization Processes in 2(2,4-Dinitrobenzyl) Pyridine Derivatives

S. Khatib,[a] S. Tal,[a,b] O. Godsi,[a] U. Peskin[a,c] and Y. Eichen[a,d,*]

[a]*Department of Chemistry, Technion—Israel Institute of Technology, Haifa 32000, Israel*
[b]*Technion Excellence Program, Technion—Israel Institute of Technology, Haifa 32000, Israel*
[c]*Lise Meitner Center for Computational Quantum Chemistry, Technion—Israel Institute of Technology, Haifa 32000, Israel*
[d]*Solid State Institute, Technion—Israel Institute of Technology, Haifa 32000, Israel*

Received 17 January 2000; revised 23 February 2000; accepted 3 March 2000

Abstract—The thermally activated **NH→CH** tautomerization process in crystals of 2(2,4-dinitrobenzyl) pyridine derivatives was investigated. The results indicate the absence of any trivial molecular structure–reactivity correlation, in contrast to what is found for similar systems in solutions. The absence of molecular structure–reactivity correlation in the crystalline state is attributed to the participation of neighboring molecules in the proton transfer process. A combined experimental and theoretical approach is presented and applied to the study of the tautomerization reaction in crystalline environments. © 2000 Elsevier Science Ltd. All rights reserved.

Introduction

Tautomerization and proton-transfer (PT) processes have been studied extensively in recent years due to their fundamental importance in many chemical and biological processes and their influence on different reaction mechanisms.[1] For example, different bacteriorhodopsin systems having the same ammonium-retinal moiety embedded in an only slightly different protein shell exhibit considerably different PT properties.[2,3] Evidence for site dependence in solid-state chemical transformations can be found also in numerous crystalline systems where a slight variation in the environment of the reactants results in a significant change in activity or in mechanism path selection.[4] Recent publications[5–7] reported the effect of the site on the determination of the absolute steric course of a photorearrangement process in crystals of different ketones and in polyenes.[8]

In most cases, rationalization of the experimental results was restricted to effects at the isolated reacting molecule level, ignoring its close packing within a solvation shell or, at most, regarding the environment as simple restriction to the molecular motion (reaction in a cage approach[9]). In other cases the effect of the crystal on the reaction kinetics and thermodynamics was rationalized in terms of a shell of rare gas atoms,[10] representing Van–der–Vaals interactions but not including specific directional interactions such as hydrogen bonds. In many other cases, such as in the case of salicylidene anylides, a straightforward structure–reactivity correlation could not be drawn for reactions in the solid state.[11]

In recent publications,[12,13] different groups compared the reactivity of several phototautomers of 2(2,4-dinitrobenzyl) pyridine derivatives in single crystals and noted the absence of any simple structure–reactivity correlation. Furthermore, in recent reports,[14] we have reported that the proton transfer kinetics of the tautomerization process in crystalline phases of 2(2,4-dinitrobenzyl)-3-methyl pyridine is sensitive to the molecular packing.

Here we report on an experimental investigation of a tautomerization process in different derivatives of 2(2,4-dinitrobenzyl) pyridine and propose a theoretical approach for modeling the reaction site effect in crystalline systems. The approach is demonstrated in the study of the proton transfer mechanism in crystals of 2(2,4-dinitrobenzyl)-3-methyl pyridine.[12]

Results and Discussion

Crystals of derivatives of 2(2,4-dinitrobenzyl) pyridine

Keywords: tautomerization; proton-transfer processes; structure–reactivity correlation.

* Corresponding author. Tel: +972-4-8293708; fax: +972-4-8233735; e-mail: chryoav@tx.technion.ac.il

PII: S0040-4020(00)00497-X

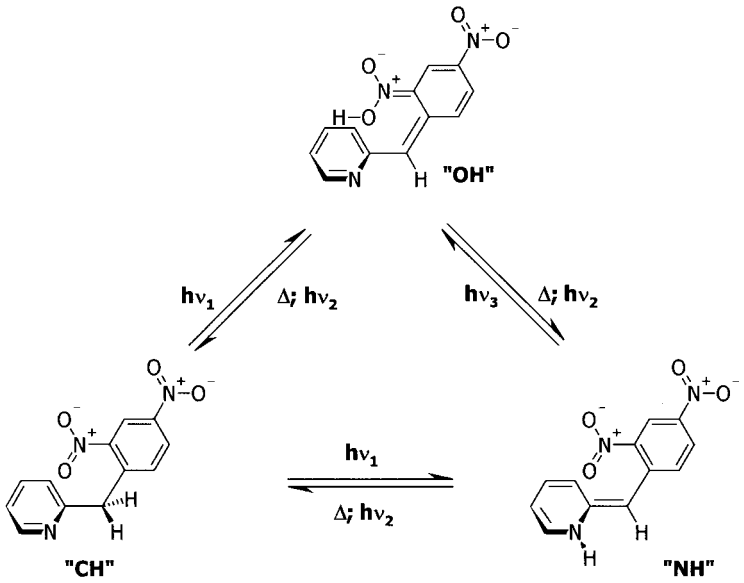

Scheme 1.

present a wealth of crystalline polymorphs of which some are photoactive while others are photoinert.[12c] The photoactive crystals develop a blue color upon UV ($\lambda<430$ nm) irradiation due to the formation of two metastable phototautomers.[11–13] Scheme 1 outlines the photoinduced and thermally activated tautomerization processes that take place in the crystalline state.[12] The possible existence of an unidentified dark metastable state was also reported.[12c,d] Typically, the blue color of the **NH** form decays homogeneously in the dark, an indication of the thermally activated **NH→CH** tautomerization process. Investigation of the thermally activated **NH→CH** process revealed a strong primary isotope effect, an indication that the proton transfer process is the rate determining step and that it is associated with only minor structural reorganization energy.[12] In crystals of 2(2,4-dinitrobenzyl) pyridine.[12,13] **1**, 2(2,4-dinitrobenzyl)-4-methyl pyridine, **2**, 2(2,4-dinitrobenzyl)-5-methyl pyridine, **3**, 2(2,4-dinitrobenzyl)-6-methyl pyridine,[12] **4**, and 1(2,4-dinitrophenyl)-1(2-pyridyl) ethane, **5**, the thermally activated **NH→CH** tautomerization process follows a monoexponential decay, while in the case of 2(2,4-dinitrobenzyl)-3-methyl pyridine,[12,14] **6**, the decay follows a biexponential curve, indicating the coexistence of two different types of **NH** phototautomers. Fig. 1 presents the Arrhenius plots for the different systems. The resulting activation energies and pre-exponential factors are summarized in Table 1. Attempts to associate the experimental activation energies for the different **NH→CH** tautomerization processes with molecular properties fail to demonstrate any obvious correlation between molecular characteristics and the observed kinetics. Intramolecular parameters for the different crystals, Table 2, also fail to reveal any consistent correlation between the molecular structure and reactivity, as was previously reported for similar DNBP derivatives in solutions.[19] Furthermore, the significant difference in the experimental activation energies observed for the **NH→CH** process in two different phases of the same molecular specie, **6**, Fig. 2, provides

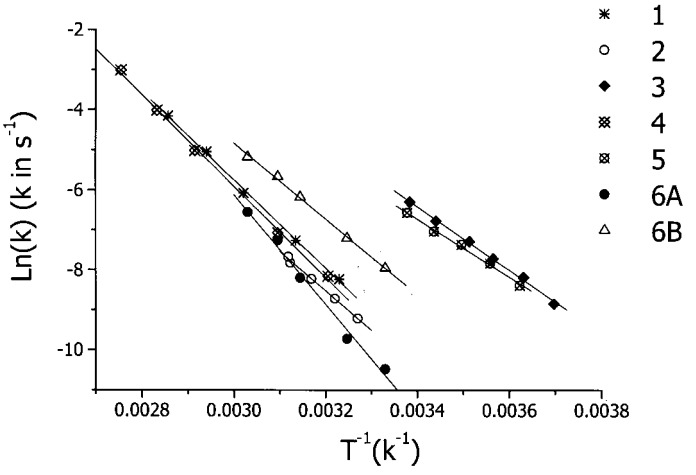

Figure 1. Arrhenius plot of the **NH** decay constants for the different crystals: **(1)** 2(2,4-dinitrobenzyl) pyridine,[13] **(2)** 2(2,4-dinitrobenzyl)-4-methyl pyridine, **(3)** 2(2,4-dinitrobenzyl)-5-methyl pyridine, **(4)** 2(2,4-dinitrobenzyl)-6-methyl pyridine,[12a] **(5)** 1(2,4-dinitrophenyl)-1(2-pyridyl) ethane, **(6a)** low temperature phase of 2(2,4-dinitrobenzyl)-3-methyl pyridine,[14a] **(6b)** high temperature phase of 2(2,4-dinitrobenzyl)-3-methyl pyridine.[14a]

Table 1. Kinetic data for the **NH→CH** process in the various systems

Crystal and phase	E_a (Kcal mol^{-1})	Log (A)
2(2,4-dinitrobenzyl) pyridine[a]	22.0±0.5	11.8±0.3
2(2,4-dinitrobenzyl)-4- methyl pyridine	19.7±0.4	10.0±0.5
2(2,4-dinitrobenzyl)-5- methyl pyridine	15.9±0.3	8.9±0.3
2(2,4-dinitrobenzyl)-6- methyl pyridine[a]	22.8±0.3	12.3±0.3
1(2,4-dinitrophenyl)-1-(2-pyridyl) ethane	14.5±0.5	7.8±0.5
2(2,4-dinitrobenzyl)-3- methyl pyridine[a] (*phase **A***)	27.4±0.8	15.2±1.1
2(2,4-dinitrobenzyl)-3- methyl pyridine[a] (*phase **B***)	18.9±0.2	10.3±0.3

[a] After Ref. 12a

strong evidence that the supramolecular structure (environment) plays an important role in controlling the tautomerization process. Chemical processes in crystalline environments differ from similar processes in solutions and gas-phase in two major points. In crystals, the molecular species usually adopt only one preferred conformation and this molecular species is confined in a well-defined static environment of neighboring molecules. Therefore, our understanding of chemical processes in solutions cannot be applied for such processes.

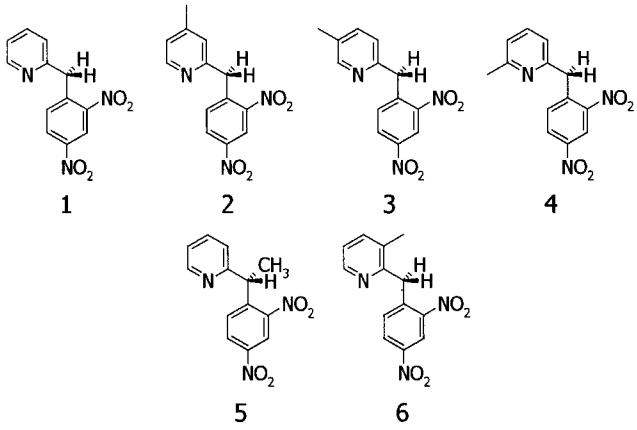

Table 2. Intramolecular parameters in crystals of 2(2,4-dinitrobenzyl) pyridine derivatives

Crystal	**1**	**2**	**3**	**4**	**5a**[a]	**5b**[a]	**6A**[b]	**6B**[b]
Pyridine–Phenyl (°)	65.1	56.9	90.7	55.0	115.1	114.8	56.10	68.31
o-Nitro-phenyl (°)	31.7	41.7	161.3	40.1	44.4	35.7	40.80	29.70
p-Nitro-phenyl (°)	12.3	15.3	167.52	12.32	7.1	6.3	14.20	8.20
N_1–H_1 (Å)	3.02	2.95	3.03	2.96	3.17	3.22	3.12	3.12
N_1–H_2 (Å)	3.06	3.12	3.04	3.09	–	–	3.01	2.95
O_1–H_1 (Å)	2.35	2.35	2.40	2.43	2.47	2.38	2.47	2.38

[a] **5a** and **5b** are the two nonequivalent molecules **5** in the same unit cell.
[b] **6A** and **6B** molecule **6** in phases **A** and **B**, respectively.

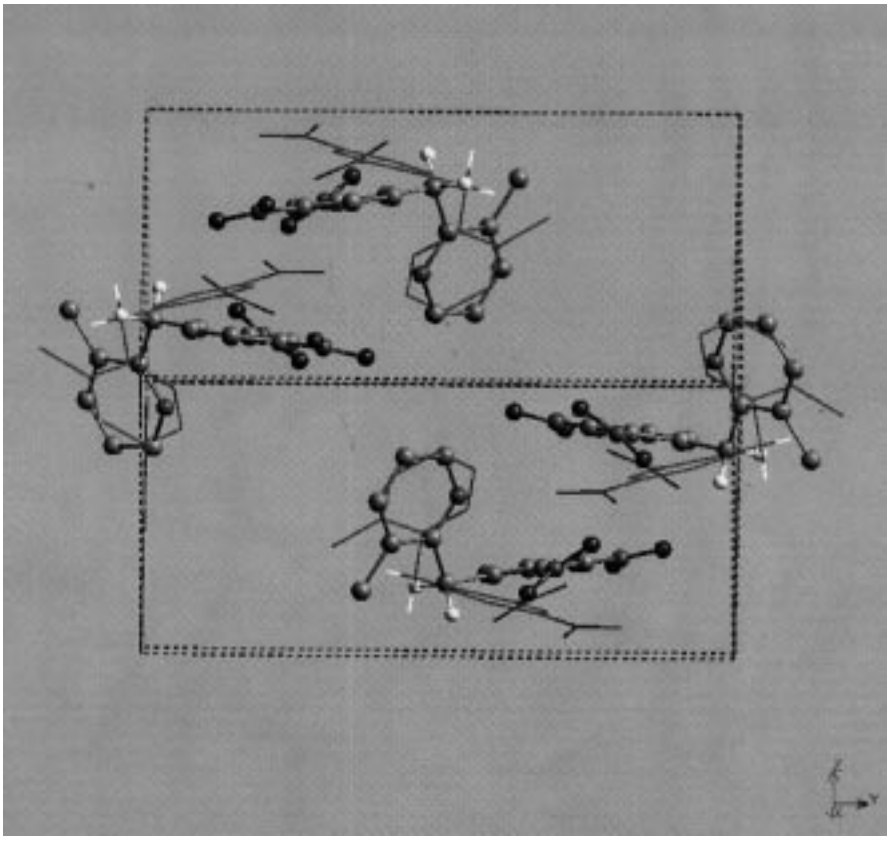

Figure 2. Crystal structure of the two different phases of 2(2,4-dinitrobenzyl)-3-methyl pyridine, phase **A** in sticks and phase **B** in balls and sticks.

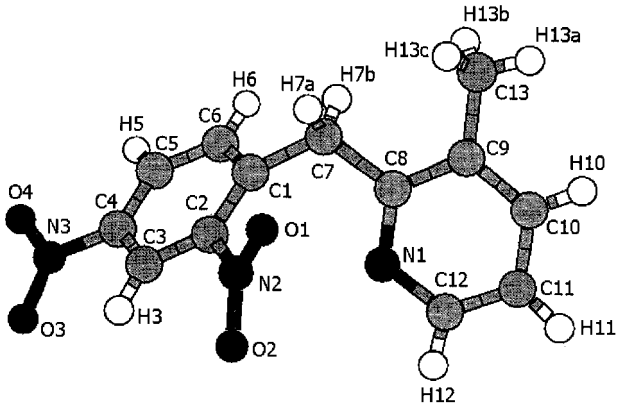

Figure 3. Atom labeling in 2(2,4-dinitrobenzyl)-3-methyl pyridine, **(6)**.

In the following, a combined theoretical–experimental approach is proposed in order to gain better understanding of chemical processes taking place in such geometrically restricted environments. As an example the case of 2(2,4-dinitrobenzyl)-3-methyl pyridine, **6**, is studied.

The theoretical approach

Two different routes were chosen for dealing with geometrically restricted systems. (a) A common approach associates the crystal with an inert cage which imposes well defined and rigid geometrical constraints on the reacting molecule. This reaction in a cage approach[9] is often used to describe reactions in rare gas matrices. Here, the assumption is that *geometrical differences* in conformation may result in different reaction paths and consequently in different activation energies for the same processes. (b) The alternative approach assumes that the crystal plays an active role in the process (an active site). In such a case, *changes in the relative orientation* between the reacting molecule and *specific functional groups* in its solvation shell may affect the ability of neighboring molecules to participate in the process. For example, in the case of 2(2,4-dinitrobenzyl)-3-methyl pyridine the neighboring molecules posses nitro and pyridine groups, that may act as Lewis bases and affect the proton transfer process. These groups are situated in close vicinity to the tautomerization reaction center. It is therefore possible that changes in the relative orientation between the reacting molecule and its neighbors will affect the ability of these molecules to participate in the tautomerization process.

In order to determine the relative importance of these different site effects, we have studied the **NH→CH** tautomerization processes in the two different phases of 2(2,4-dinitrobenzyl)-3-methyl pyridine, **6**. This system provides a favorable test case for a computational study of site effects for the following reasons: (a) the structure of the thermodynamically stable tautomer and its environment is known experimentally in both phases; (b) systematic errors associated with the choice of specific computational models should not be expressed in the difference between the reaction paths. These errors are minimized since the two different phases differ only slightly in terms of intra- and intermolecular parameters (the same molecule in a slightly different conformation). Nevertheless, the large number of atoms ($>10^2$) required for the construction of a realistic model for the molecule embedded in its environment (vide infra) currently limits our quantum chemical description to semi-empirical Hartree–Fock calculations.[15]

The theoretical treatment is based on the following scheme. (a) The crystallographic structure of the product (the thermally stable tautomer **CH**) is revealed experimentally from X-ray crystallography. All computational treatments are based on this structure. (b) The reactants (the **NH** tautomers) are photogenerated in high dilution. Therefore, they are isolated from one another and *are surrounded by a large number of non reacting molecules*. Thus, the perturbation to the crystalline structure during the reaction is assumed to be nil. (c) Local site effects control the stability of the reactants. Collective effects such as coupling to H-bond networks or coupling to floppy global lattice phonons are ignored within this approximation. (d) Local site effects can be represented approximately by a compact model for the reacting molecule in its solvation shell. Within this model, lattice constraints are represented artificially by fixing selected atoms of the molecular skeleton at their crystallographic coordinates. Naturally, the goal of such an approach is to minimize the number of geometrically constrained atoms in the reacting molecule in order to allow molecular motion along the tautomerization process. (e) The free motion of side groups, which liberate significantly in the crystal (such as methyl and nitro groups[17]), is not restricted artificially during the tautomerization process.

Reaction mechanism

Tautomerization processes in derivatives of DNBP are associated with a three-center proton transfer reaction profile and can take a direct path, **NH→CH**, or an indirect path through **OH** intermediate states, **NH→OH→CH**. Previous semi-empirical and DFT calculations suggest that reactions along both paths involve the *o*-nitro group either as an active intermediate, **OH**, or as a chaperon that escorts the moving proton through a hydrogen bond, thus lowering the barrier along the direct path.[16] While the **OH** tautomer was not yet observed in the two phases of 2(2,4-dinitrobenzyl)-3-methyl pyridine, it was identified as a metastable state in many analogous systems.[12,13] Therefore, both the direct and indirect pathways should be considered in the theoretical treatment.

Model A: a single constrained molecule

As a first model, a single geometrically constrained molecule is considered. At this level, the major conformational difference between the two phases of 2(2,4-dinitrobenzyl)-3-methyl pyridine, **6**, is expressed by the pyridine–phenyl interplanar angle, being 56.1° in the low-temperature phase (phase A) and 68.3° in the high-temperature phase (phase B).[14] This difference between the two phases was represented by fixing two carbon atoms on each ring (atoms **C2**, **C5**, **C11** and **C13** in Fig. 3) to their Cartesian crystallographic coordinates. All other molecular parameters were optimized using semi-empirical MOPAC (PM3-SCF) electronic structure calculations. The resulting optimized geometry in each phase constitutes the

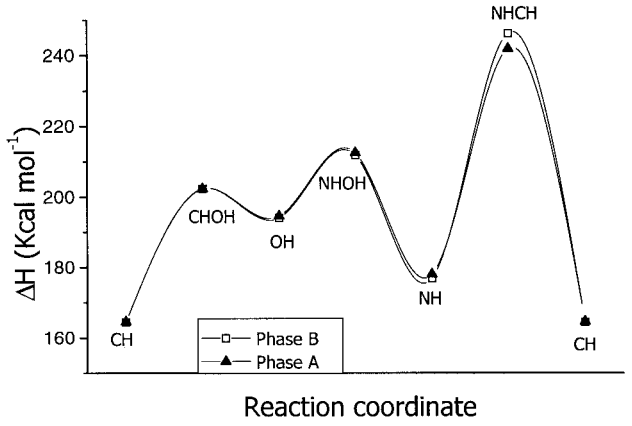

Figure 4. Calculated reaction profiles (circles and squares for phases **A** and **B** respectively) for the direct and indirect **NH→CH** reactions within a model of a single constrained molecule (the full line is for illustration, see text for constrained atoms).

compact model for the thermally stable **CH** tautomer. The crystallographic structure of the **NH** phototautomer and the transition-state, **TS**, are experimentally unknown. However, according to our basic model assumptions, the interplanar ring in the **NH** phototautomer is kept as in the thermally stable **CH** phototautomer during the tautomerization process.[18] Therefore, the structure of the **NH** phototautomer was determined within the same geometrical constraints as above. Once the constrained structures of the reactant **NH** and the product **CH** tautomers were realized, the transition states for the direct **NH→CH** and the indirect **NH→OH→CH** tautomerization reactions were determined using a saddle point search algorithm[19] subjected to the same geometrical constraints. Unlike in the case of unconstrained molecule in the gas phase, the **TS** geometry is not an extreme point on the full **3*N***-6 dimensional molecular potential energy surface. Assuming that ***n*** atoms were fixed to their crystallographic locations (where ***n*** >1), the **TS** is a saddle-point on a 3 (***N*–*n***) dimensional subsurface of the remaining active degrees of freedom. In order to characterize the transition state frequencies, a constrained normal mode analysis was carried out at the saddle-point geometry. Denoting the Cartesian coordinates of ***N*** atoms as $X=(x_1,x_2,\ldots,x_{3N})$, the nuclear Hamiltonian at the saddle point is approximated (harmonically) as Eq. (1)

$$H_{\text{nuc}} = \tfrac{1}{2}\dot{X}^{\text{t}}M\dot{X} + \tfrac{1}{2}X^{\text{t}}FX \qquad (1)$$

where M is a diagonal matrix whose non-zero elements are the nuclei masses, $M_{i,j}=m_i\delta_{i,j}$, F the Hessian matrix in Cartesian coordinates and X^{t} denotes the transposed coordinates vector. The mass-weighted normal mode force constants are the eigenvalues of f (see Eq. (2)).

$$f = \begin{bmatrix} \frac{1}{\sqrt{m_1}} & & & & \\ & \ddots & & & \\ & & \frac{1}{\sqrt{m_i}} & & \\ & & & \ddots & \\ & & & & \frac{1}{\sqrt{m_{3N}}} \end{bmatrix} \cdot F \cdot \begin{bmatrix} \frac{1}{\sqrt{m_1}} & & & & \\ & \ddots & & & \\ & & \frac{1}{\sqrt{m_i}} & & \\ & & & \ddots & \\ & & & & \frac{1}{\sqrt{m_{3N}}} \end{bmatrix} \qquad (2)$$

In order to impose the lattice constraints on the normal modes in consistency with the constrained electronic structure calculations, we associate each constrained atom with an artificial large mass, i.e. we let $m_i \to \infty$ (i=1,2,…,***n***), so that the elements of the corresponding ith row and ith column of f approach zero, Eq. (3).

$$f \underset{m_i\to\infty}{\to} \begin{bmatrix} & & 0 & & \\ & & \vdots & & \\ 0 & \ldots & 0 & \ldots & 0 \\ & & \vdots & & \\ & & 0 & & \end{bmatrix} \qquad (3)$$

Diagonalization of this artificial mass-weighted Hessian matrix yields only (**3*N*−3*n***) non-zero force constants (eigenvalues), associated with the normal modes of the active (**3*N*−3*n***) nuclear degrees of freedom.

Fig. 4 presents the energy profile calculated for a single isolated constrained molecule along the different reaction paths. The model of *a single constrained molecule* fails to reproduce the relative stability of the different phases as was observed experimentally. One barrier was found along the **NH→CH** direct path. Along the indirect path, two barriers were allocated, corresponding to the two consecutive processes, **NH→OH** and **OH→CH**. All calculated values for the different paths are depicted in Table 3. These calculations, based on the model of *a single constrained molecule*, show no significant difference between the two phases in terms of the energetics along the indirect reaction path and a somewhat lower barrier in phase A along the direct path. Similar results were obtained when the constraints were placed on atoms (**C1**, **C4**, **C8** and **C11** in Fig. 3), Table 3. In this case, the molecules are allowed some motion along the ring axes. These results do not agree with the experimentally measured difference in the

Table 3. Calculated electronic energies (corrected for zero point energy) (kcal mol^{-1}) along the **NH→CH** reaction path for a single constrained molecule

	Phase **A** C2,C5,C11,C13	Phase **B** C2,C5,C11,C13	Phase **A** C1,C4,C8,C11	Phase **B** C1,C4,C8,C11
CH	164.62	164.50	162.06	163.03
CHOH	202.35	202.38	205.32	204.17
OH	194.55	194.01	196.61	197.60
NH–OH	212.43	211.79	203.41	205.56
NH	178.04	176.91	177.93	179.45
NH–CH	241.95	246.34	217.25	217.18

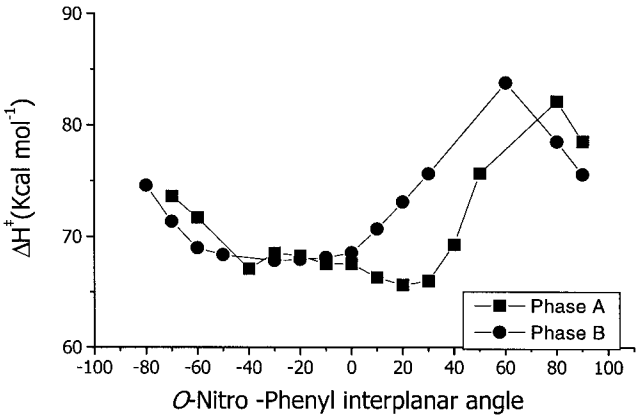

Figure 5. Calculated activation energy for a single constrained molecule in the two phases as a function of the (constrained) interplanar angle between the *o*-nitro and the phenyl ring (the full line is for illustration, see text for constrained atoms).

reaction activation energy between the two phases ($E_{aB}-E_{aA}=-8.45$ kcal mol^{-1}).

The role of the *o*-nitro group

Another possible difference in the crystalline structure of 2(2,4-dinitrobenzyl)-3-methyl pyridine, **6**, is expressed in the libration of the *o*-nitro group of the reacting molecule within the crystal lattice. Differences in crystal packing may limit the motion of the *o*-nitro group and thus affect the ability of this group to participate in the process. We have therefore investigated the influence of fixing the *o*-nitro-phenyl interplanar angle on the calculated reaction barrier along the direct path. The angle was set and frozen by fixing the nitrogen atom (N2) and an oxygen atom (O1) to their positions. All other parameters in the calculations were identical to the ones reported for the first model of an isolated constrained molecule (**C2**, **C5**, **C11** and **C13** in Fig. 3). Fig. 5 depicts the calculated activation enthalpy as a function of the *o*-nitro-pheny interplanar angle. As can be seen from Fig. 5, the ability of the static *o*-nitro group to assist in the proton transfer along the direct path is angle-dependent. Additionally, the different molecular conformations originating from the different phases exhibit different behavior. Although the same calculation cannot be easily performed on the indirect path due to problems originating from imposing constrains on the *o*-nitro group it is expected that libration (the dynamics of the nitro group) plays an even more important role along the indirect path. Detailed investigation of the relative orientation of the reacting molecule with respect to its first shell neighbors in the two different phases show a significant difference in the distance between the *o*-nitro group of the reacting molecule and atoms of neighboring molecules, Fig. 6. Additionally, there is a significant difference between the crystals of the two phases in terms of the distance between different Lewis bases and protons of neighboring molecules and the groups participating in the process (active proton, nitrogen atom of the pyridine ring, *o*-nitro group) within the reacting molecule. It is therefore desirable to include the effects of the environment within a more realistic model.

Model B: Compact models for the crystalline environment

A major effort in our approach is to determine the number of neighbors, which are required for a reliable representation of the reaction site with a minimal number of constrained atoms in the reacting molecule. The following selection process is proposed, and tested for the 2(2,4-dinitrobenzyl)-3-methyl pyridine, **6**, system. The constraints, based on the crystallographic structure of the **CH** tautomer, were set as follows: All skeleton atoms of selected neighboring molecules were fixed, assuming only negligible perturbation to their structure due to the tautomerization process. Hydrogen atoms (of which the crystallographic coordinates are not accurate[20]) and nitro groups, which exhibit significant libration in the crystal, were not constrained. In the reacting molecule, selected atoms were fixed to their crystallographic coordinates in order to further restrict the motion. All other coordinates were optimized computationally, using MOPAC PM3-SCF. The structures of the **NH** and the different **OH** tautomers were determined as above within the same constraints. The calculated atomic coordinates of the reacting molecule were compared to the crystallographic structure, and a measure for the difference

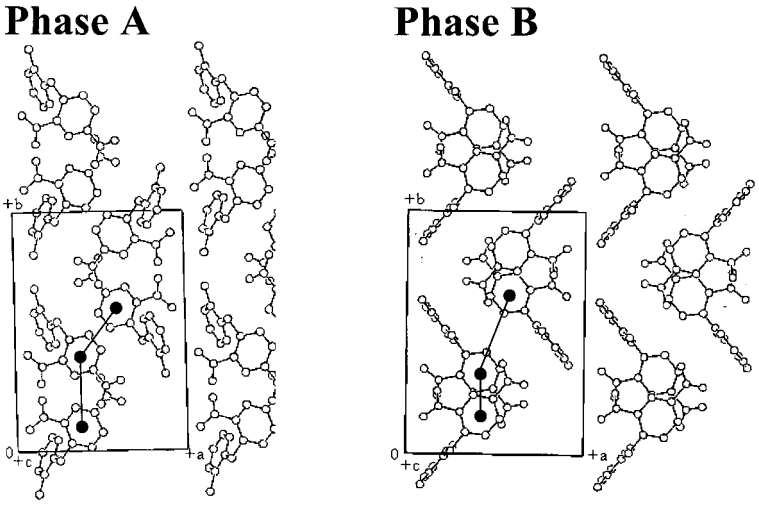

Figure 6. Supramolecular arrangement of **6** in phases **A** (left) and **B** (right) viewed along the *c* axis.

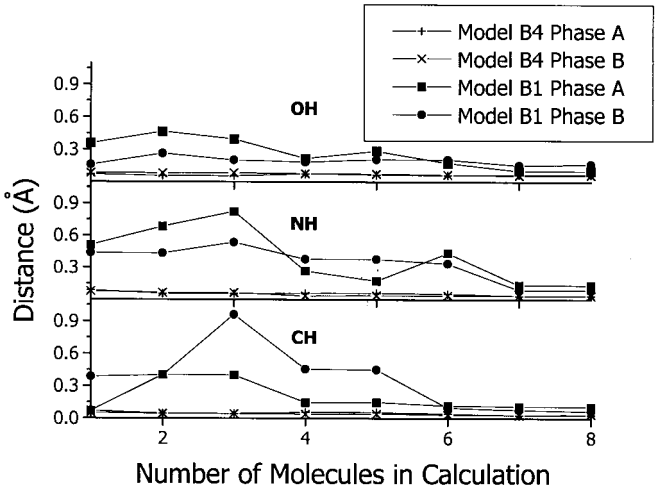

Figure 7. A plot of the distance, ***D***, as a function of the number of neighboring molecules in the cases of four (+— phase **A**, ×— phase **B**) and one (■— phase **A**, ●— phase **B**) constrained atoms. See Table 4 for the specific identity of each molecule and text for constraint atoms.

between the model calculation and the experimental structure was defined as the distance *D*, Eq. (4), where *N* is the number of heavy (non H) atoms in the reacting molecule and *X* is the vector of Cartesian atomic coordinates.

$$D = \frac{1}{N}\sqrt{\sum_{i=1}^{3N}(X_i^{\mathrm{cal}} - X_i^{\mathrm{exp}})^2} \qquad (4)$$

Fig. 7 depicts the distance, *D*, as a function of the number of neighboring molecules for different constraints imposed on the reacting molecule, Table 4. When four atoms are constrained in the reacting molecule so that the inter-ring angle is fixed (Model B4, **C1**, **C4**, **C8**, **C11** in Fig. 3) the molecular geometry is essentially fixed by the constraints. Consequently, the structure of the reacting molecule, as expressed by the distance, *D*, is insensitive to the number and identity of the neighboring molecules. When only a single atom in the reacting molecule is constrained (Model B1, **C7** in Fig. 3), the distance, *D*, becomes dependent on the number and the identity of the neighboring molecules. Nevertheless, five to seven neighboring molecules are sufficient in order to converge the influence of the molecular environment on the geometry of the reacting molecule. This holds for the thermodynamically stable **CH** tautomer as well as for the **NH** and **OH** phototautomers. Minimizing the number of constrained atoms in the reacting molecule is crucial for a reliable representation of the reaction path. Therefore, calculations that take into account higher number of neighbors and less intramolecular constraints are favorable. Another measure of the reliability of the computational model is the comparison of the differences in enthalpy between the two phases. Fig. 8 depicts the calculated lattice enthalpy (per molecule) in the different models as a function of the number of molecules. The lattice energy calculated for phase A is lower than the one calculated for phase B, regardless of the particular model. This is in consistency with the experimental data.[14] Interestingly, the enthalpies of formation calculated for a single isolated molecule adopting the conformation at the two phases do not differ significantly. This degeneration is lifted, however, upon the introduction of a molecular environment.

These thermodynamic studies demonstrate that it is possible to represent realistically the local influence of the lattice on the reacting molecule, by a relatively small number of neighbors. A detailed calculation of the reaction path and the activation energy within such a compact model is currently in progress.

Conclusions

Surroundings effects on intra-molecular PT processes in crystals of 2(2,4-dinitrobenzyl) pyridines were studied and characterized in terms of energetics and mechanism. A combined experimental–theoretical approach based on

Table 4. The distances, *D*, in the two models, as a function of the number of molecules in the calculation.

Molecule added to the model	Symmetry	***D*** (Å)			
		Model B4 Phase **A**	Model B4 Phase **B**	Model B1 Phase **A**	Model B1 Phase **B**
1	x, y, z	0.07	0.05	0.07	0.38
2	$x, y, 1+z$	0.04	0.04	0.40	0.40
3	$x, y, 1-z$	0.04	0.04	0.40	0.96
4	$x, (1/2)-y, (1/2)+z$	0.05	0.04	0.15	0.46
5	$-x, (1/2)+y, (1/2)-z$	0.05	0.04	0.15	0.45
6	$-x, -y, -z$	0.04	0.03	0.12	0.10
7	$1-x, -y, 1-z$	0.03	0.03	0.11	0.08
8	$-x, -y, 1-z$	0.03	0.03	0.11	0.07

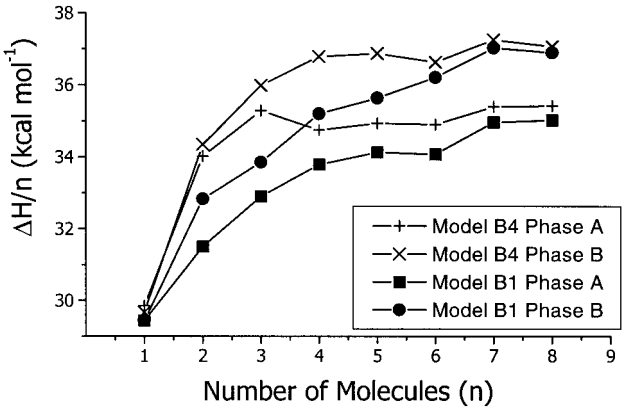

Figure 8. Calculated lattice enthalpy (per molecule) as a function of the number of molecules: (a) four constrained atoms (**C1**, **C4**, **C8** and **C11**); (b) one constrained atom (**C7**).

constrained compact models for the reaction site was introduced and applied to the study of proton transfer in 2-(2,4-dinitrobenzyl)-3-methyl pyridine. It was found that differences in the molecular packing in two crystalline phases affect significantly the calculated energy profile along the different reaction paths, as suggested by the thermodynamic and kinetic measurements. The insight gained by the different models implies that the intramolecular *o*-nitro group activates the direct **NH→CH** PT reaction and that interactions between this group and neighboring molecules in the reaction site affect dramatically the PT reaction profile.

Presently, the proposed theoretical approach relies on experimental crystallographic data and it is limited to ordered single crystals whose stable structure can be determined experimentally. It is also assumed that the PT reaction is in high dilution, so that the crystal structure does not change during the reaction. The main advantage of the present approach is the ability to treat specific molecular interactions in the reaction site and to characterize their effects on reaction energetics and mechanism. However, the model is currently limited to short range local interactions and neglects long-ranged (global) effects that are likely to be of important in some cases. Even so, when only the first solvation shell is considered, the number of atoms is large (typically $>10^2$) and the present calculations were limited to the semi-empirical Hartree–Fock level. We anticipate that optimized choices of the constraints would enable us to obtain smaller realistic models, which will enable calculations at ab initio levels.

Experimental

Materials

All reagents were used as received unless noted. 2-benzyl pyridine derivatives were prepared by $[ph_3P]_4Pd$ catalyzed heterocoupling between benzylzincbromide and the appropriate 2-bromopyridine derivative. 2-benzyl-3-methyl pyridine,[12a] 2-benzyl-6-methyl pyridine,[12a] 2(2,4-dinitrobenzyl) -3-methyl pyridine[12a] and 2(2,4-dinitrobenzyl)-6-methyl pyridine[12a] were prepared according to previously published procedures.

Apparatus

Time dependent absorption spectra were measured on a Cary 1E (Varian) spectrophotometer. Time dependent optical density curves were recorded using a PC-controlled, home-made, spectrometer having a Nd:YAG laser (λ=355 nm) or a Mercury lamp equipped with an appropriate filter (UG11, Schott) as the exciting light beam. The detection system consisted a liquid nitrogen cooled CCD (Princeton Instruments) connected to a 150i spectrograph (Acton Research) or a photomultiplier system. A liquid nitrogen cooled optical cryostat (Oxford, Instrument, DN 1704) equipped with a temperature controller (Lake Shore 330, Cryotronics) was used to regulate the temperature of the samples. All experiments were performed in high dilution, photoexciting only a very small ($\ll$0.1%) part of the molecules in the crystal. Semi-empirical calculations were carried out using a modified MOPAC93 package.[15] The code was modified in order to enable a constrained transition-state search and constrained normal mode analysis.

2-Benzyl-4-methyl pyridine. Benzyl bromide (2.68 g, 0.014 mol) was added dropwise to a suspension of activated zinc dust (3.8 g, 0.058 mol) in dry THF under argon atmosphere. As soon as the flask reaches room temperature, the solution was filtered under inert atmosphere and added to a mixture of 2-bromo-4-methyl pyridine (2 g, 0.011 mol) and $[ph_3P]_4Pd$ (0.1 g, 0.086 mmol) in 25 ml dry THF under argon. The mixture was stirred overnight then evaporated and filtered using a short alumina column. The product was isolated as a colorless viscous oil, 2.1 g, 99% yield. ^{1}H NMR($CDCl_3$): d_{ppm}; 2.25(s, 3H); 4.09(s, 2H); 6.9(s, 2H); 7.25(m, 5H); 8.4(d, 1).

2-Benzyl-5-methyl pyridine. Benzyl bromide (2.17 g, 0.011 mol) was added dropwise to a suspension of activated Zn dust (3.8 g, 0.058 mol) in dry THF under argon atmosphere. As soon as the flask reaches room temperature, the solution was filtered under inert atmosphere and added to a mixture of 2-bromo-5-methyl pyridine (2 g, 0.011 mol) and $[ph_3P]_4Pd$ (0.1 g, 0.086 mmol) in 25 ml dry THF under argon. The mixture was stirred overnight then evaporated and filtered using a short alumina column. The product was isolated as a colorless viscous oil, 1.7 g, 80% yield. ^{1}H NMR($CDCl_3$): d_{ppm} 2.26(s, 3H); 4.09(s, 2H); 6.95(d, 1H); 7.2(m,6H); 8.3(s, 1H).

1-Phenyl-1(2-pyridine) ethane. Butyl lithium 2.5 M solution in hexane (5.5 ml) were added dropwise to 2-benzylpyridine (1.9 g, 11.24 mmol) in dry THF under argon atmosphere at −30°C. Methyl iodide (1 ml, 16 mmol) was added after 20 min and the solution was allowed to reach room temperature. After stirring the solution for three hours the THF was evaporated and the product was chromatograph (alumina, ether/hexane 30:70) to yield 1.97 g (96%) of the product ^{1}H NMR($CDCl_3$): d_{ppm}=1.66(d, 3H); 4.26(q, 1H); 7.1(m, 2H); 7.2(m, 5H); 7.53(t, 1H); 8.5(d, 1H).

2(2,4-Dinitrobenzyl)-4-methyl pyridine (2). 25 ml of cold sulfuric acid were added dropwise to 2-benzyl-4-methyl

pyridine, (1 g, 5.46 mmol) at −10°C, and stirred for several minutes to ensure complete dissolution of the pyridine derivative. 6 ml HNO_3 (100%, fuming) were added to the mixture and the solution was allowed to reach room temperature. After stirring the solution for three hours at room temperature, the solution was poured on ice made basic using ammonia solution and extracted with three portions of dichloromethane. The combined organic layers were concentrated and chromatograph (alumina, ether/hexane 20:80) to yield 0.8 g (53%) of the product as colorless crystals. Mp: 64.96°C; MS: (EI) 272; ^{1}H NMR($CDCl_3$): d_{ppm}; 2.3(s, 3H); 4.52(s, 2H); 6.9(d, 1H); 7.05(s, 1H); 7.62(d, 1H); 8.27(d, 1H); 8.33(d, 1H); 8.8(s, 1H). ^{13}C NMR ($CDCl_3$): d_{ppm}; 21.29; 41.18; 120.49; 123.40; 124.68; 127.15; 129.64; 134.56; 141.56; 146.97; 148.47; 149.62; 156.88.

2(2,4-Dinitrobenzyl)-5-methyl pyridine (3). 25 ml of cold sulfuric acid were added dropwise to 2-benzyl-5-methyl pyridine, (1 g, 5.46 mmol) at −10°C, and stirred for several minutes to ensure complete dissolution of the pyridine derivative. 6 ml HNO_3 (100%, fuming) were added to the mixture and the solution was allowed to reach room temperature. After stirring the solution for three hours at room temperature, the solution was poured on ice made basic using ammonia solution and extracted with three portions of dichloromethane. The combined organic layers were concentrated and chromatograph (alumina, ether/hexane 20:80) to yield 1.1 g (73%) of the product as colorless crystals. Mp: 97.56°C; MS: (-DCI) 272.9, 256.0, 242.9. ^{1}H NMR($CDCl_3$): d_{ppm}; 4.5(s, 3H); 4.52(s, 2H); 7.1(d, 1H); 7.4(d, 1H); 7.6(d, 1H); 8.2(s, 1H); 8.3(d, H); 8.8(s, 1H). ^{13}C NMR($CDCl_3$): d_{ppm}; 17.99; 40.47; 120.18; 123.03; 126.84; 131.63; 134.28; 137.55; 141.338; 146.66; 149.21; 149.88; 153.722.

1(2,4-Dinitrobenzyl)-1(2-pyridine) ethane (5). 25 ml of cold sulfuric acid were added dropwise to 1-phenyl-1-(2-pyridyl) ethane, (1 g, 5.46 mmol) at −10°C, and stirred for several minutes to ensure complete dissolution of the pyridine derivative. 6 ml HNO_3 (100%, fuming) were added to the mixture and the solution was allowed to reach room temperature. After stirring the solution for three hours at room temperature, the solution was poured on ice made basic using ammonia solution and extracted with three portions of dichloromethane. The combined organic layers were concentrated and chromatograph (alumina, ether/hexane 20:80) to yield 1.1 g (75%) of the product as colorless crystals. Mp: 63.36°C; MS: (EI) 272; ^{1}H NMR($CDCl_3$): d_{ppm}; 1.74(d, 3H); 4.87(q, 1H); 7.1(t, 1H); 7.23(d, 1H); 7.62(t, 1H); 7.86(d, 1H); 8.32(d, 1H); 8.53(d, 1H); 8.62(s, 1H). ^{13}C NMR($CDCl_3$): d_{ppm}; 21.08; 41.53; 119.50; 122.155; 122.96; 126.51; 131.81; 136.86; 146.07; 146.617; 161.156.

Acknowledgements

This research was supported by the US–Israel Binational Science Foundation (BSF), the Israel Science Foundation (ISF), the Israeli Ministry of Science and the foundation for promotion of research at the Technion.

References

1. (a) Lanyi, J. K. *J. Biol. Chem.* **1997**, *272*, 31209–31212. (b) Hirst, J.; Duff, J. L. C.; Jameson, G. N. L.; Kemper, M. A.; Burgess, B. K.; Armstrong, F. A. *J. Am. Chem. Soc.* **1998**, *120*, 7085–7094. (c) Mitchell. P. *Nature* **1961**, *191*, 144. (d) Williams, R. J. P. *Biochim. Biophys. Acta* **1991**, *1058*, 71–74. (e) Babcock, G. T.; Wikström, M. *Nature* **1992**, *356*, 301–309.

2. For a special issue dedicated to retinal proteins see *Isr. J. Chem.* **1995**, *35*, 193–515.

3. (a) Brauchle, C.; Hammp, N.; Osterhelt, D. *Adv. Mater.* **1991**, *3*, 420–428. (b) Osterhelt, D.; Brauchle, C.; Hampp, N. *Q. Rev. Biophys.* **1991**, *24*, 425478.

4. Stoeckenios, W.; Bogomolni, R. A. *Annu. Rev. Biochem.* **1982**, *51*, 587–616.

5. Choi, T.; Peterfy, K.; Khan, S. I.; Garcia-Garibay, M. A. *J. Am. Chem. Soc.* **1996**, *118*, 12477–12478.

6. Liebovittch, M.; Olovson, G.; Scheffer, J. R.; Trotter, J. *J. Am. Chem. Soc.* **1997**, *119*, 1462–1463.

7. Liebovittch, M.; Olovson, G.; Scheffer, J. R.; Trotter, J.; Ramamurthy, V.; Sundarababu, G. *J. Am. Chem. Soc.* **1996**, *118*, 1219–1220.

8. Amarendra, K. V.; Venkatesan, K. *J. Chem. Soc. Perkin Trans. 2* **1991**, 829–835.

9. (a) Zimmerman H. E.; Zuram, M. J. *J. Am. Chem. Soc.* **1989**, *111*, 2358–2361. (b) Alimi, R.; Gerber, R. B.; McCaffrey, J. R.; Kunz, H.; Schwentner, N. *Phys. Rev. Lett.* **1992**, *69*, 856–859.

10. Zimmerman, H. E.; Sebek, P.; Zhu, Z. *J. Am. Chem. Soc.* **1998**, *120*, 8549–8550.

11. *Photochromism: Molecules and Systems. Studies in Organic Chemistry 40*; Durr, H., Bouas-Laurant, H., Eds.; Amsterdam, 1990, Chapter 17, and references therein.

12. a) Schrel, M.; Haarer, D.; Fischer, J.; Decian, A.; Lehn, J. M.; Eichen, Y. *J. Phys. Chem.* **1996**, *100*, 16175–16186. (b) Eichen, Y.; Lehn, J.-M.; Scherl, M.; Haarer, D.; Fischer, J.; DeCian, A.; Corval, A.; Trommsdorff, H. P. *Angew. Chem., Int. Ed. Engl.* **1995**, *34*, 2530–2533. (c) Khatib, S.; Botoshansky, M.; Eichen, Y. *Acta Crystallogr.* **1997**, *B53*, 306–316. (d) Ziane, O.; Casalegno, R.; Corval, A. *Chem. Phys.* **1999**, *250*, 199–206. (e) Sousa, J. A.; Loconti, J. D. *Science* **1964**, *146*, 397–398.

13. Sixl, H.; Warta, R. *Chem. Phys.* **1985**, *94*, 147–155.

14. (a) Eichen, Y.; Botoshansky, M.; Peskin, U.; Scherl, M.; Haarer, D.; Khatib, S. *J. Am. Chem. Soc.* **1997**, *119*, 7167–7168. (b) Schmidt, A.; Kababya, S.; Appel, M.; Khatib, S.; Botoshansky, M.; Eichen, Y. *J. Am. Chem. Soc.* **1999**, *121*, 11291–11299.

15. Stewart, J. J. P. MOPAC 93 manual; Fujitsu Ltd, Tokyo, Japan, 1993.

16. (a) Frank, I.; Marx, D.; Parrinello, M. *Phys. Chem. A* **1999**, *103*, 7341–7344. (b) Frank, I.; Grimme, S.; Peyerimhoff, S. D. *J. Phys. Chem.* **1996**, *100*, 16187–16194.

17. Seff, K.; Trueblood, K. N. *Acta Crystallogr. B* **1968**, *24*, 1406–1415.

18. This is based on the observation that the two rings are sandwiched between two rings of neighboring molecules. In contrast, side groups are generally loosely bound to distant atoms or unbound.

19. Dewar, M. J. S.; Healy, E. F.; Stewart, J. J. P. *J. Chem. Soc., Faraday Trans. II* **1984**, *3*, 227–233.

20. Hamilton, W. C. *J. Chem. Ed.* **1968**, *45*, 296–303.